Small Platinum Clusters in Zeolites: A Density Functional Study of CO Adsorption on Electronically Modified Models

Anna Maria Ferrari, Konstantin M. Neyman, Thomas Belling, Markus Mayer, and Notker Rösch*

Lehrstuhl für Theoretische Chemie, Technische Universität München, D-85747 Garching, Germany

Received: August 19, 1998; In Final Form: November 2, 1998

Very small transition metal particles can be stabilized inside zeolite cavities. Both electron-enriched and electron-deficient encapsulated metal species have been proposed on the basis of experimental data. In this work, structure and adsorption properties of the cluster Pt_4, in both neutral and electronically modified forms, have been studied computationally with the help of a scalar-relativistic density functional method. The species Pt_4^+ has been chosen to represent the case of a metal particle interacting with an electron attracting zeolite host; likewise, Pt_4^- has been taken to mimic the effect of an electron-donating host. Adsorption of CO probe molecules at on-top, bridge, and 3-fold hollow sites of the moieties Pt_4, Pt_4^+, and Pt_4^- has been investigated to determine a relationship between the cluster charge and the C−O vibrational frequency shift $\Delta\omega$(CO). The chemical effect of electron-donor and electron-acceptor species on the electronic structure of the Pt_4 clusters and on the properties of adsorbed CO probes has been also explicitly taken into account by employing various models XPt_4CO (X = Na, Na^+, NH_3). Properties of adsorbed CO probe molecules were calculated to be rather sensitive to the electronic state and the adsorption site of the Pt_4 particles, in line with experimental findings. A linear correlation between the effective charge of the metal cluster and the adsorption-induced vibrational frequency shift $\Delta\omega$(CO) has been found for CO adsorbed at on-top positions.

Introduction

Highly dispersed transition metal particles supported on oxides constitute an important class of heterogeneous catalysts.[1] In particular, molecular sieves and zeolites are often used successfully to support very small metal moieties.[2] Transition metal particles of a few atoms, as stabilized in zeolite cages, exhibit peculiar intrinsic electronic properties because of their small size; yet, as a result of interactions with the zeolite framework, they may undergo a considerable change in electronic structure and thus in their catalytic behavior. Both electron-deficient and electron-enriched states of metal species in zeolite cavities were proposed on the basis of experimental data.[3] Electron-deficient states were rationalized as being due to interactions of the metal particles with Brønsted acid sites of zeolites,[2,4] while the existence of electron-enriched metal species was attributed to the influence of the basic framework oxygen centers.[3] Furthermore, electron-donor or electron-acceptor species and charge-balancing cations, present in the zeolite cages, can also affect the electronic structure and properties of small encapsulated metal particles.

Owing to the importance of transition metals and especially platinum as catalysts in many industrial processes,[1] much work has been devoted during the past decade to the characterization of small metal particles entrapped in zeolite cages.[3−14] By use of extended X-ray adsorption fine structure (EXAFS) spectroscopy, very small encaged metal clusters of 4−10 atoms were detected in zeolites.[8,9,15−18] CO molecules have been widely used to probe structural and electronic properties of supported metal particles benefiting from the high sensitivity of the C−O stretching frequency ω(CO) to the oxidation states of metal particles,[19,20] their size,[11,14,21] and the strength of metal−support interactions.[22] Correlations of the electronic state and size of the clusters with the C−O vibrational frequency shift $\Delta\omega$(CO) have been put forward.[10,11,14] In addition to infrared (IR) spectroscopy, several other methods including X-ray photoelectron spectroscopy[23,24] (XPS) and catalytic tests, such as competitive hydrogenation of benzene and toluene,[3,25] were employed to characterize the electronic state of metal species confined to zeolite cavities. However, the interpretation of these experimental data is often ambiguous because measured values of adsorption parameters characterizing supported moieties, e.g., the frequency shift $\Delta\omega$(CO), are usually the result of more than one effect. As a rule, when the electronic states of encapsulated metal species change because of interactions with the support, so do their sizes and shapes. It is a valuable advantage of quantum chemical studies that they allow the separation of different effects. For instance, computational investigations can help to elucidate how such features of metal clusters as their size and shape on one hand and the electronic state on the other hand affect the bonding and vibrational properties of CO probe molecules that are adsorbed on different sites of the metal substrate.

This work is devoted to the analysis of adsorption properties (binding energies, geometrical parameters, electronic structure, vibrational frequencies) of CO probe molecules bound to small platinum clusters; of particular interest is how these properties depend on the charge of the cluster and on the adsorption site. For this purpose we have studied computationally, using a density functional (DF) approach, the adsorption of a CO molecule on neutral and electronically modified Pt_4 clusters. Three cases have been considered: CO adsorbed (i) on a neutral cluster Pt_4, (ii) on a positively charged cluster Pt_4^+ mimicking

* Corresponding author.

10.1021/jp983446z CCC: $18.00
Published on Web 12/19/1998

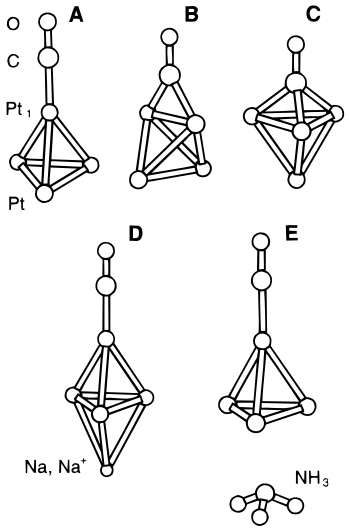

Figure 1. Configurations of CO adsorbed on Pt_4 clusters: on top **A**, bridge **B**, 3-fold hollow **C** as well as on top of the clusters Na/Pt_4 or Na^+/Pt_4 **D** and NH_3/Pt_4 **E**.

the action of an electron-attracting support, and (iii) on a negatively charged cluster Pt_4^- modeling the effect of an electron-donor support. We employ naked electronically modified clusters to model encapsulated species that become (partially) charged as a result of interaction with the zeolite frameworks. Of course, this model strategy can only furnish a rather approximate description of real systems. The charge interval of Pt_4 clusters considered here, ranging from +1 to −1 au, is probably too large for such small species. For these reasons the calculated results have to be taken with due care. For instance, in the case of closely lying excited states the calculated ground state of the charged Pt_4 clusters would not necessarily coincide with the ground electronic (and spin) state of the encaged Pt_4 species, and one has to discuss the choice of the appropriate model ground state. Fortunately, in most of the cases studied below, the results calculated for different electron configurations of Pt_4/CO complexes that fall into a narrow energy interval above the cluster model ground state are not significantly different with respect to pertinent properties. This provides additional justification for the models employed in the present study.

The interaction properties have been analyzed in detail as a function of CO coordination sites (on-top, bridge, and 3-fold hollow; Figure 1) and of the electronic charge of the cluster. To validate electronically modified metal clusters as models of moieties interacting with electron-attracting or electron-donor centers in zeolites, we have also explicitly taken into account the chemical effect of electron-donor and electron-acceptor species on the electronic structure of Pt_4 clusters and on the interaction properties of an adsorbed CO probe. In these extended models, an NH_3 molecule or a sodium atom has been coordinated to the cluster Pt_4 to simulate electron-donor effects experienced in zeolites; an Na^+ cation has been utilized to mimic the interaction with the electron-acceptor species of a host.

Computational Method and Models

The calculations have been carried out at the DF level of theory with the help of a scalar-relativistic variant of a linear combination of Gaussian-type orbitals density functional method (LCGTO-DF)[26,27] as implemented in the new program ParaGauss for parallel computers.[28−30] Spin-polarized calculations have been performed in order to account for the magnetic nature of the substrate clusters under study. Large and flexible basis sets have been utilized for expanding the Kohn−Sham orbitals. For Pt atoms, a (19s,14p,10d,5f) Gaussian-type basis set[31] has been extended by two s (0.01, 0.193 936 734), three p (0.030 931 116 8, 0.077 327 792, 0.193 319 48), two d (0.057 630 721 6, 0.144 076 804), and two f exponents (0.167 922 231 3, 0.671 688 925). The resulting set of functions (21s,17p,12d,7f) was contracted to [10s,8p,5d,3f]. This basis set has previously been used in calculations of CO adsorption on Pt surfaces.[32,33] For C, N, and O atoms, basis sets of the type (9s,5p,2d) → [5s,4p,2d] have been adopted.[34,35] A basis set of the type (12s,8p,2d) → [6s,5p,2d] (with d exponents 0.122 and 0.01825) was used for Na.[36,37] H atoms have been described by the basis set (6s,2p) → [3s,2p].[34,35] All contractions were of generalized form. The auxiliary fitting basis sets employed to represent the electron charge density have been constructed by properly scaling the s and p exponents of the orbital basis sets in a standard fashion.[26] For Pt atoms, only every second p-type exponent has been used in constructing d(r^2)-type fitting functions. Furthermore a set of five p- and five d-type polarization exponents located on every atom have been added to the fitting basis set.[32] The fitting functions are used to calculate the classic Coulomb potential of the electron−electron interaction. The exchange-correlation energy and the matrix elements of the exchange-correlation potential have been evaluated by numerical integration.[38,39]

The geometry of the various molecular systems has been optimized automatically using analytical energy gradients.[40] Harmonic vibrational frequencies have been derived from force constants that were calculated numerically within a finite difference approach. These calculations were carried out employing the local spin density (LSD) approximation.[41]

The accuracy of the LSD functional for describing properties of Pt_n/CO adsorption complexes was assessed by comparison with reference calculations with the help of the gradient-corrected BP functional (Becke's exchange functional[42] in combination with Perdew's correlation functional[43]). CO adsorption on-top and on 3-fold hollow sites has been represented by the models Pt/CO and Pt_3/CO, respectively. As shown in Table 1, the results of LSD and BP calculations for distances Pt−Pt and Pt−C agree within 0.05 Å. For the C−O distance the agreement is within 0.01 Å. Also the adsorption-induced shifts of the C−O stretching frequency $\Delta\omega$(CO) calculated at

TABLE 1: Comparison of Various Observables of the Models Pt/CO and Pt_3/CO with CO on Top and on the 3-Fold Hollow Site, Respectively, Calculated with LSD and BP Functionals[a]

	Pt_3/CO		Pt/CO	
	LSD	BP	LSD	BP
r(Pt−Pt)	2.558	2.607		
r(Pt−C)	2.005	2.043	1.750	1.774
r(C−O)	1.199	1.208	1.156	1.165
BE	2.99	1.88	4.54	3.69
BE(BP//LSD)[b]		1.86		3.68
BE_{BSSE}	2.85	1.73	4.43	3.58
BE_{BSSE} (BP//LSD)[b]		1.70		3.57
ω(Pt−CO)	493	463	625	624
ω(CO)	1743	1688	2108	2060
$\Delta\omega$(CO)	−419	−420	−54	−48

[a] Interatomic distances r in Å, binding energy BE of CO to Pt and Pt_3 moieties in eV, also corrected for the basis set superposition error, BE_{BSSE}, intermolecular Pt−CO stretching frequency ω(Pt−CO), intramolecular C−O stretching frequency ω(CO), and the corresponding shift $\Delta\omega$(CO) in cm^{-1} relative to the values calculated for the free CO molecule (LSD 2162 cm^{-1}, BP 2108 cm^{-1}). [b] Energy calculated at the BP level for the geometry determined in the LSD approximation.

TABLE 2: Symmetry, Electronic Configuration,[a] Corresponding Orbital Occupation, and Assigned Electronic State for All Systems under Study

system	symmetry	configuration	state[b]
Pt_4	T_d	$15a_1^{\uparrow 1}15a_1^{\downarrow 1}1a_2^{\uparrow 1}1a_2^{\downarrow 1}12e^{\uparrow 2}12e^{\downarrow 2}13t_1^{\uparrow 3}12t_1^{\downarrow 3}27t_2^{\uparrow 1}26t_2^{\downarrow 3}$	$^5T_2$
Pt_4^+	T_d	$15a_1^{\uparrow 1}15a_1^{\downarrow 1}1a_2^{\uparrow 1}1a_2^{\downarrow 1}12e^{\uparrow 2}12e^{\downarrow 2}13t_1^{\uparrow 3}12t_1^{\downarrow 3}26t_2^{\uparrow 3}26t_2^{\downarrow 3}$	$^4A_1$
Pt_4^-	T_d	$15a_1^{\uparrow 1}15a_1^{\downarrow 1}1a_2^{\uparrow 1}1a_2^{\downarrow 1}12e^{\uparrow 2}12e^{\downarrow 2}13t_1^{\uparrow 3}12t_1^{\downarrow 3}27t_2^{\uparrow 2}26t_2^{\downarrow 3}$	$^6T_1$
Pt_4/CO (on top)	C_{3v}	$46a_1^{\uparrow 1}46a_1^{\downarrow 1}14a_2^{\uparrow 1}13a_2^{\downarrow 1}52e^{\uparrow 2}52e^{\downarrow 1}$	^3E
Pt_4/CO (bridge)	C_{2v}	$58a_1^{\uparrow 1}57a_1^{\downarrow 1}26a_2^{\uparrow 1}26a_2^{\downarrow 1}40b_1^{\uparrow 1}39b_1^{\downarrow 1}40b_2^{\uparrow 1}40b_2^{\downarrow 1}$	$^3B_1$
Pt_4/CO (hollow)	C_{3v}	$45a_1^{\uparrow 1}45a_1^{\downarrow 1}14a_2^{\uparrow 1}14a_2^{\downarrow 1}52e^{\uparrow 2}52e^{\downarrow 2}$	$^1A_1$
Pt_4^+/CO (on top)	C_{3v}	$46a_1^{\uparrow 1}46a_1^{\downarrow 1}14a_2^{\uparrow 1}13a_2^{\downarrow 1}52e^{\uparrow 2}51e^{\downarrow 2}$	$^4A_1$
Pt_4^+/CO (bridge)	C_{2v}	$57a_1^{\uparrow 1}57a_1^{\downarrow 1}26a_2^{\uparrow 1}26a_2^{\downarrow 1}40b_1^{\uparrow 1}39b_1^{\downarrow 1}40b_2^{\uparrow 1}40b_2^{\downarrow 1}$	$^2B_1$
Pt_4^+/CO (hollow)	C_{3v}	$45a_1^{\uparrow 1}45a_1^{\downarrow 1}14a_2^{\uparrow 1}14a_2^{\downarrow 1}52e^{\uparrow 2}52e^{\downarrow 1}$	^2E
Pt_4^-/CO (on top)	C_{3v}	$46a_1^{\uparrow 1}46a_1^{\downarrow 1}14a_2^{\uparrow 1}13a_2^{\downarrow 1}52e^{\uparrow 2}52e^{\downarrow 2}$	$^2A_2$
Pt_4^-/CO (bridge)	C_{2v}	$58a_1^{\uparrow 1}57a_1^{\downarrow 1}26a_2^{\uparrow 1}25a_2^{\downarrow 1}41b_1^{\uparrow 1}39b_1^{\downarrow 1}41b_2^{\uparrow 1}40b_2^{\downarrow 1}$	$^6B_1$
Pt_4^-/CO (hollow)	C_{3v}	$46a_1^{\uparrow 1}45a_1^{\downarrow 1}14a_2^{\uparrow 1}14a_2^{\downarrow 1}52e^{\uparrow 2}52e^{\downarrow 2}$	$^2A_1$
Na/Pt_4	C_{3v}	$45a_1^{\uparrow 1}44a_1^{\downarrow 1}14a_2^{\uparrow 1}14a_2^{\downarrow 1}52e^{\uparrow 2}51e^{\downarrow 2}$	$^4A_2$
Na^+/Pt_4	C_{3v}	$44a_1^{\uparrow 1}44a_1^{\downarrow 1}14a_2^{\uparrow 1}14a_2^{\downarrow 1}52e^{\uparrow 2}51e^{\downarrow 2}$	$^3A_2$
NH_3/Pt_4	C_{3v}	$44a_1^{\uparrow 1}44a_1^{\downarrow 1}14a_2^{\uparrow 1}13a_2^{\downarrow 1}53e^{\uparrow 1}51e^{\downarrow 2}$	^5E
Na/Pt_4/CO	C_{3v}	$49a_1^{\uparrow 1}49a_1^{\downarrow 1}14a_2^{\uparrow 1}13a_2^{\downarrow 1}53e^{\uparrow 2}53e^{\downarrow 2}$	$^2A_2$
Na^+/Pt_4/CO	C_{3v}	$49a_1^{\uparrow 1}49a_1^{\downarrow 1}14a_2^{\uparrow 1}13a_2^{\downarrow 1}53e^{\uparrow 2}53e^{\downarrow 1}$	^3E
NH_3/Pt_4/CO	C_{3v}	$49a_1^{\uparrow 1}49a_1^{\downarrow 1}14a_2^{\uparrow 1}13a_2^{\downarrow 1}53e^{\uparrow 2}53e^{\downarrow 1}$	^3E

[a] Only the highest occupied spin orbitals of each irreducible representation are reported. [b] Assigned state based on the (high spin) electron configuration determined by the occupation numbers that result from a spin-polarized calculation. The assignment is unique in all cases considered.

the LSD and BP levels agree rather well, to better than 10 cm^{-1}. The results of the two functionals for the intermolecular Pt−CO stretching frequency ω(Pt−CO) differ by at most 30 cm^{-1} (Table 1). The tendency of LSD approximation to overestimate binding energies is well established.[44] Nevertheless, agreement between the binding energies evaluated with the help of BP and combined BP//LSD approaches is remarkably close, to about 0.02 eV (Table 1). (In the combination strategy BP//LSD, the binding energy is evaluated at the BP level, but for the equilibrium geometry it is optimized at the LSD level.) Thus, all binding energies in this work have been computed according to this economic and accurate BP//LSD procedure;[45] they were corrected for the basis set superposition error (BSSE) as estimated by the counterpoise method.[46]

No precise experimental data on the actual sizes, structures, and shapes of very small platinum clusters encapsulated in zeolites are available, although Pt species of 5−12 atoms were identified by EXAFS spetroscopy.[9,18] However, there is EXAFS evidence that iridium clusters can be entrapped in Na−Y zeolites as tetrahedral Ir_4 moieties.[16] By analogy, the four-atom cluster Pt_4 in tetrahedron-like shape has been chosen in the present study as a model for conceivable small encaged platinum species. This cluster shape has been calculated as the most stable one for free Pt_4.[47] It represents also the smallest species that exhibits the three most common adsorption sites: on-top, bridge, and 3-fold hollow (Figure 1). Full geometry optimizations of these three types of adsorption complexes CO/Pt_4 have been carried out under C_{3v}, C_{2v}, and C_{3v} symmetry constraints, respectively. Na, Na^+, and NH_3 species have been attached to the Pt_4 cluster as ligands occupying a 3-fold position; in these models, the CO adsorbate has been placed in an on-top fashion at the opposite side of the cluster (structures **D** and **E** of Figure 1). On-top adsorption has been experimentally found to be the most favorable for CO on platinum clusters and surfaces in the low-coverage regime.[3−24] Geometry optimizations for all the complexes containing Na, Na^+, and NH_3 species, with or without adsorbed CO, were carried out under the C_{3v} symmetry constraint. T_d symmetry has been imposed to the neutral and charged Pt_4 reference clusters.

Results and Discussion

CO Adsorbed on Pt_4. The free Pt_4 cluster (T_d) is characterized by a Pt−Pt intermetal distance, r(Pt−Pt) = 2.509 Å, that is considerably shorter than the corresponding distance observed in Pt metal bulk, r(Pt− Pt) = 2.775 Å.[48] This contraction of the intermetal distance is not unexpected, since a similar trend has been computed for small gold and palladium clusters.[49,50] The resulting electronic ground state of Pt_4 is $^5T_2$; see Table 2 for further details. (Notice that in this work the electronic states are assigned on the basis of the electronic configurations, thereby neglecting any possible spin contamination.) At the MR-SDCI level the Pt_4 ground state turned out to be $^3T_1$,[47] while we found a $^5T_2$ ground state even at the BP level of calculation. However, in our calculations the $^5T_2$ state is only slightly more stable than the $^3T_1$ state, by 0.09 at the LSD level and by 0.19 eV the BP level.

Selected calculated parameters that characterize the interaction of a CO probe molecule with a neutral Pt_4 cluster are collected in Table 3 for all three adsorption geometries of CO investigated, on-top, bridge, and 3-fold hollow (Figure 1). The corresponding electronic configurations and assigned ground states are reported in Tables 2 and 3. Pt_4/CO complexes where CO is adsorbed on top or at the bridge site result in triplet states (^3E and $^3B_1$, respectively), whereas a singlet state $^1A_1$ was computed for CO bound to the 3-fold hollow site. In all three adsorption complexes, the number of unpaired spins is reduced compared to the case of the free cluster ($^5T_2$). This adsorption-induced spin quenching of transition metal clusters has been extensively studied elsewhere.[51] In a recent investigation the on-top interaction of CO on a Pt(111) surface was described by Pt_4 and Pt_{13} model clusters at the CASSCF and MP2 levels, employing a 10-electron pseudopotential to describe the Pt atom at the adsorption site and a one-electron pseudopotential for all other Pt atoms.[52] In that work ^2E and ^4E ground states were computed for Pt_4/CO and Pt_{13}/CO, respectively.

The pertinent geometric parameters change considerably in comparison to the free fragments, in particular, the intramolecular distance r(C−O) and the intermetal Pt−Pt distances involving atoms in direct contact with the CO molecule r(Pt_1−Pt_1) and r(Pt_1−Pt). This indicates that the fragments CO and Pt_4 undergo substantial interactions. The intermolecular distance r(Pt_1−C) increases with the number of metal atoms coordinated at the adsorption site, i.e., from on-top to bridge to hollow sites; the computed Pt_4−CO binding energies BE show a concomitant but opposite trend (Table 3). The present computed values r(Pt_1−C) = 1.825 Å, r(C−O) = 1.159 Å, BE = 2.50 eV for

TABLE 3: Calculated Properties of the Neutral Complex Pt_4/CO and the Charged Complexes Pt_4^+/COand Pt_4^-/CO Complexes with CO on Top, on the Bridge, and on the Hollow Sites (See Also Figure 1)[a]

	Pt_4/CO			Pt_4^+/CO			Pt_4^-/CO				
	on top	bridge	hollow	on top	bridge	hollow	on top	bridge	bridge	hollow	hollow
configuration[g]	a_2e^3	a_1b_1	e^4	a_2e^2	b_1	e^3	a_2e^4	$a_1a_2b_1b_1b_2$	$a_1b_1b_2$	e^4a_1	e^4e^1
electronic state	^3E	$^3B_1$	$^1A_1$	$^4A_1$	$^2B_1$	^2E	$^2A_2$	$^6B_1$	$^4A_2$	$^2A_1$	^2E
r(C−O)[b]	1.159	1.185	1.216	1.140	1.179	1.197	1.178	1.193	1.196	1.216	1.230
z(Pt_1−C)[c]	1.825	1.369	1.190	1.896	1.299	1.241	1.790	1.372	1.353	1.279	1.138
r(Pt_1−C)	1.825	1.937	1.981	1.896	1.920	1.996	1.790	1.950	1.935	2.010	1.980
r(Pt_1−Pt)[d]	2.589	2.570	2.521	2.540	2.550	2.505	2.629	2.534	2.592	2.531	2.512
r(Pt−Pt)	2.481	2.461		2.483	2.490		2.487	2.525	2.445		
r(Pt_1−Pt_1)		2.734	2.743		2.828	2.708		2.771	2.766	2.686	2.805
BE(CO)[e]	3.37	3.16	3.02	2.68	2.63	2.33	3.72	3.56	3.32	3.09	2.93
	(3.21)	(3.02)	(2.89)	(2.53)	(2.49)	(2.21)	(3.55)	(3.41)	(3.17)	(2.95)	(2.80)
BE(CO)[f]	2.50	2.07	1.78	1.88	1.60	1.11	2.81	2.56	2.22	1.88	1.66
	(2.35)	(1.89)	(1.58)	(1.63)	(1.43)	(0.92)	(2.65)	(2.38)	(2.04)	(1.69)	(1.46)
ω(Pt−CO)	565	450	373	447	432	370	607	456	466	382	366
ω(CO)	2050	1831	1596	2120	1860	1701	1961	1796	1779	1610	1518
$\Delta\omega$(CO)[b]	−112	−331	−566	−42	−302	−461	−201	−366	−383	−552	−646
$d\mu/dr$[b]	−2.90	−1.86	−1.62	−2.43	−1.65	−1.48	−3.50	−1.96	−1.89	−1.63	−1.53
$d\mu_\sigma/dr$[b]	1.20	1.15	1.19	1.12	1.13	1.14	1.43	1.16	1.17	1.16	1.15
$d\mu_\pi/dr$[b]	−4.10	−3.07	−2.85	−3.55	−2.83	−2.65	−4.92	−3.13	−3.12	−2.82	−2.72

[a] Distances r and z in Å, binding energies BE of CO to the platinum cluster in eV (BSSE corrected values BE_{BSSE} in parentheses), Pt_4−CO vibrational stretching frequency ω(Pt−CO), C−O stretching frequency ω(CO) and its adsorption-induced shift $\Delta\omega$(CO) in cm^{-1}, CO dynamic dipole moment $d\mu/dr$ and its σ and π components $d\mu_\sigma/dr$ and $d\mu_\pi/dr$ in au. [b] Free CO: r(CO) = 1.134 Å, ω(CO) = 2162 cm^{-1}, $d\mu/dr = -0.66$ au, $d\mu_\sigma/dr = 0.36$ au, $d\mu_\pi/dr = -1.02$ au. [c] Height of the carbon atom above the top atom or layer of the Pt_4 cluster measured along the normal of the Pt_3 subunit. [d] r(Pt−Pt) for free clusters in T_d symmetry: 2.509 Å (Pt_4), 2.517 Å (Pt_4^-), and 2.502 Å (Pt_4^+). [e] Computed at the LSD level (see also Computational Method and Models). [f] Computed at BP//LSD level (see also Computational Method and Models). [g] See also Table 2.

CO on-top and r(Pt_1−C) = 1.937 Å, r(C−O) = 1.185 Å, BE = 2.07 eV for CO at the bridge site are in qualitative agreement with DF values from cluster model calculations for CO adsorbed on a Pt(100) surface, r(Pt_1−C) = 1.87 Å, r(C−O) = 1.16 Å, BE = 1.46 eV for CO on-top and r(Pt_1−C) =2.02 Å, r(C−O) = 1.18 Å, BE = 1.30 eV for CO on a bridge site,[32] as well as with experimental distances on Pt surfaces, r(Pt−C) = 1.85 Å for CO on-top and 2.08 Å for CO at a bridge site.[53] Slightly different parameters were computed at CASSCF and MP2 levels:[52] r(Pt_1−C) = 1.9−2.0 Å, r(C−O) = 1.11−1.15 Å, BE = 0.9−1.2 eV (cf. Table 3).

The on-top site is calculated to be the preferred binding site among the three possibilities studied for Pt_4; the 3-fold hold site exhibits the weakest bonding interaction (Table 3). On-top adsorption was already computed to be the most favorable on Pt surfaces using model clusters[33] and model slab band structure calculations.[54]

The intermolecular stretching frequency ω(Pt−CO) decreases with the number of Pt atoms to which CO is coordinated (Table 3), in agreement with the elongation of the r(Pt_1−C) distance and the reduction of the CO binding energy. The computed value ω(Pt−CO) = 565 cm^{-1} for on-top CO (Table 3) is between the DF results calculated in the model cluster approach for CO adsorbed on the Pt(100) surface,[33] ω(Pt−CO) = 464 cm^{-1}, and for platinum monocarbonyl PtCO, ω(Pt−CO) = 680 cm^{-1}.[32]

The calculated C−O vibrational frequency ω(CO) is one of the most interesting features of the adsorption complexes because it can be directly compared with experimental values measured by IR spectroscopy. For all Pt_4/CO complexes considered, the computed C−O stretching frequency is red-shifted with respect to free CO (Table 3). The shift $\Delta\omega$(CO) increases by about 200 cm^{-1} each in absolute value when going from on-top to the bridge and further to the 3-fold site, concomitantly with the number of Pt atoms to which CO is coordinated as well as with the C−O bond elongation. These results are consistent with experimental data for CO adsorbed on platinum surfaces[55−60] where $\Delta\omega$(CO) values in the range −50 to −70 cm^{-1} and −170 to −190 cm^{-1} have been found for on-top and bridge species, respectively. For CO adsorbed on platinum clusters of the size of about 10 Å supported on inert substrates such as SiO_2 and Al_2O_3, the C−O frequency is measured to be red-shifted compared to the free molecule, by about −70 cm^{-1}; under low coverage conditions it moves to even lower values, with $\Delta\omega$(CO) = −83 to −86 cm^{-1}.[61−64] A red shift of the C−O frequency by about −70 cm^{-1} has also been observed for on-top adsorption on zeolite-encaged massive platinum moieties with an estimated particle diameter of 40 Å, for which the influence of the host is expected to be small.[7,10,14,65] These experimental values compare reasonably well with the computed result, $\Delta\omega$(CO) = −112 cm^{-1} (Table 3), if one takes into account that the metal cluster size can affect $\Delta\omega$(CO) by several tens of wavenumbers.[11] The present result compares well with previously computed values obtained with a gradient-corrected density functional, $\Delta\omega$(CO) = −98 cm^{-1},[33] and at the CASSCF and MP2 levels, $\Delta\omega$(CO) = −88 and −61 cm^{-1}, respectively.[52]

TABLE 4: Calculated Bond Length and Vibrational Frequency of Neutral CO and Its Various Cationic and Anionic States with One Electron Either Removed from the 4σ, 5σ, or 1π Orbitals or Added to the $2\pi^*$ Orbital

	CO	CO^+ ($5\sigma^{-1}$)	CO^+ ($4\sigma^{-1}$)	CO^+ ($1\pi^{-1}$)	CO^- ($2\pi^{*+1}$)
r(C−O), Å	1.134	1.120	1.160	1.256	1.228
ω(CO), cm^{-1}	2162	2239	2014	1520	1668
$\Delta\omega$(CO), cm^{-1}		+77	−148	−642	−494

Before turning to an analysis of adsorption-induced changes of the CO valence orbitals and the concomitant shift of the CO stretching frequency, we display in Table 5 spectroscopic constants calculated for free CO, as well as for various cationic and anionic configurations that are intended to mimic electronic states of coordinated CO rather than free CO^+ or CO^- free species. (Experimentally, the anionic configuration $CO^-(2\pi^{*1})$ is observed as a resonance only[66] with a negative electron affinity of −1.5 eV,[66] which is in line with our computed value of −1.96 eV.) Ionization from the 5σ MO results in a positive frequency shift $\Delta\omega$(CO) = 77 cm^{-1} (cf. the experimental value[66]

TABLE 5: Mulliken σ and π Populations and Charges q Calculated for the Clusters Pt_4/CO, Pt_4^+/CO, and Pt_4^-/CO, in au

	Pt_4/CO			Pt_4^+/CO			Pt_4^-/CO				
	on top	bridge	hollow	on top	bridge	hollow	on top	bridge[a]	bridge[b]	hollow[a]	hollow[b]
σ(C)	4.31	4.24	4.18	4.34	4.19	4.18	4.29	4.25	4.26	4.21	4.19
σ(O)	5.17	5.19	5.16	5.19	5.19	5.17	5.16	5.18	5.18	5.16	5.15
σ(CO)	9.48	9.42	9.34	9.53	9.38	9.35	9.45	9.43	9.44	9.37	9.34
π(C)	1.59	1.77	1.94	1.48	1.81	1.91	1.67	1.78	1.77	1.87	1.94
π(O)	2.97	3.00	3.07	2.86	2.95	2.98	3.08	3.06	3.09	3.10	3.11
π(CO)	4.56	4.77	5.01	4.34	4.76	4.89	4.75	4.84	4.86	4.97	5.05
q(C)	0.10	−0.02	−0.12	0.18	0.02	−0.08	0.04	−0.03	−0.03	−0.09	−0.11
q(O)	−0.15	−0.19	−0.23	−0.04	−0.14	−0.15	−0.24	−0.24	−0.25	−0.26	−0.28
q(CO)	−0.04	−0.21	−0.35	0.13	−0.12	−0.23	−0.19	−0.27	−0.28	−0.34	−0.39
q(Pt_1)	−0.25	−0.07	0.10	−0.06	0.37	0.84	−0.39	−0.44	−0.58	−0.48	−0.64
q(Pt)	0.30	0.28	0.24	0.93	0.75	0.39	−0.47	−0.28	−0.14	−0.18	0.03

[a] Corresponding to the $^6B_1$ and $^2A_1$ electronic states for the bridge and hollow sites, respectively. [b] Corresponding to the $^4A_2$ and ^2E electronic states for the bridge and hollow sites, respectively.

TABLE 6: Calculated Properties of the Complexes X/Pt_4 and X/Pt_4/CO (X = Na, Na^+, NH_3)[a] as Well as of the Model Clusters Pt_4^q/CO (q = −0.35, 0.68 au; See Text) with CO Adsorbed on Top (See Figure 1)

	Na/Pt_4	Na^+/Pt_4	NH_3/Pt_4	Na/Pt_4/CO	$Pt_4^{-0.35}$/CO	Na^+/Pt_4/CO	$Pt_4^{+0.68}$/CO	NH_3/Pt_4/CO
configuration[d]	e^2a_1	e^2	$a_2e^2e^1$	a_2e^4	$a_2e^{3.35}$	a_2e^3	$a_2e^{2.32}$	a_2e^3
electronic state[d]	$^4A_2$	$^3A_2$	^5E	$^2A_2$		^3E		^3E
r(C−O)				1.165	1.166	1.148	1.146	1.158
r(Pt_1−CO)				1.791	1.809	1.838	1.867	1.828
r(Pt_1−Pt)	2.515	2.487	2.510	2.613	2.607	2.570	2.555	2.599
r(Pt−Pt)	2.536	2.594	2.518	2.504	2.481	2.502	2.482	2.481
r(Pt−X)	2.834	2.912	3.028	2.804		2.942		3.354
BE(X)[b]	2.42	1.30	0.35					
	(2.32)	(1.21)	(0.l6)					
BE(X)[c]	2.06	1.00	−0.04					
	(1.97)	(0.91)	(−0.20)					
BE(CO)[b]				3.44	3.53	3.83	2.85	3.45
				(3.27)	(3.37)	(3.67)	(2.69)	(3.29)
BE(CO)[c]				2.62	2.57	2.90	2.01	2.61
				(2.46)	(2.43)	(2.75)	(1.86)	(2.46)
ω(Pt−CO)				583	589	529	489	547
ω(CO)				2016	2022	2098	2099	2046
$\Delta\omega$(CO)				−146	−140	−64	−63	−116
q(CO)				−0.101	−0.100	0.056	0.074	−0.035
q(Pt_1 + Pt)	−0.165	0.595	−0.213	−0.181	−0.250	0.543	0.606	−0.102
q(X)	0.165	0.405	0.213	0.282		0.402		0.137

[a] Distances r in Å, binding energies BE(X) of X to Pt_4 and BE(CO) of CO to X/Pt_4 in eV (BSSE corrected binding energies in parentheses), Pt−CO vibrational stretching frequency ω(Pt−CO), C−O stretching frequency ω(CO), and the corresponding shift $\Delta\omega$(CO) relative to the free CO molecule in cm^{-1}, Mulliken charges q in au. [b] Computed at LSD level (see also Computational Method and Models). [c] Computed at BP//LSD level (see also Computational Method and Models). [d] See also Table 2.

of 44 cm^{-1}), which indicates the slightly antibonding nature of this orbital. Removal of an electron from the bonding 4σ MO induces a vibrational red shift of −148 cm^{-1}. When an electron is removed from the 1π MO or added in the 2π* MO, much larger values of the red shift $\Delta\omega$(CO) result, −642 and −494 cm^{-1}, respectively. From these results one expects, in line with a previously published correlation,[26] that π back-donation affects the C−O stretching mode significantly stronger than the σ donation.

The bonding of CO to a transition metal species is commonly described by the Blyholder donor−acceptor mechanism[67] with electron donation from the adsorbate to unoccupied metal orbitals through the CO 5σ molecular orbital (MO) and back-donation from the d_π metal orbitals to the unoccupied 2π* level of CO.[67] The 4σ and 1π MOs of CO, to a smaller extent, also participate in the donation.[68−70] This picture of CO−metal bonding has been analyzed and modified with the help of the constrained space orbital variation (CSOV) procedure.[32,52,71−73] This unconventional bonding analysis applied to Pt−CO monocarbonyl[33] and to CO adsorbed on top of Pt_4 and Pt_{13} cluster models[52,74] helped to identify basically four interaction channels: (a) Pauli repulsion, (b) σ donation, (c) π back-donation, and (d) metal substrate polarization. Pauli repulsion between the frozen electronic densities of the adsorbate and the metal cluster causes a large positive shift of ω(CO); the other two mechanisms, σ donation and π back-donation, turn the "initial" blue shift into an overall red shift, the latter contribution being larger. The link existing between π back-donation and CO vibrational properties was theoretically tested in a wide number of different systems. These include metal carbonyl complexes, small metal−CO molecules, and CO on metal surfaces.[26,71−75] Although $\Delta\omega$(CO) was found to be dominated by π back-donation, the binding energy BE(CO) was found to result from a delicate balance of all four contributions.[32,52] This finding indicates that the two quantities BE(CO) and $\Delta\omega$(CO) depend in different ways on the aforementioned four interaction contributions.

In the present study, we analyzed the changes of the electronic structure of the probe molecule CO, induced by the different number of Pt atoms at the adsorption sites, with the help of a Mulliken population analysis (Table 6). Recall that a Mulliken analysis is not free of artifacts, in particular when extended basis sets are employed.[75] Nevertheless, this scheme often provides a useful albeit rough estimate of the charge transfer that accompanies bond formation. One can see that donation does not vary much with the adsorption site (Table 6). However,

according to the data in Table 4, even considerable changes in the 5σ population should not significantly affect the CO stretching frequency. By the same token, the small metal admixtures to the 4σ and 1π MOs, which represent adsorbate-to-substrate donation, should entail small contributions to the overall red shift of ω(CO). From the results of Table 5, even moderate changes in the π population of CO are expected to substantially alter the C−O vibrational frequency (see Tables 3 and 6). (Note that the CSOV analysis[52] indicates that the CO → Pt_4 donation is mainly via the σ channel; therefore, it is possible to qualitatively correlate the variations of π populations displayed in Table 5 with the amount of π back-donation.) Finally, we notice that π back-donation increases with the number of Pt atoms of the adsorption site, and indeed, the red shift of ω(CO) increases as well (Tables 3 and 6).

The IR intensity of the C−O band is proportional to the square of the dynamic dipole moment $(d\mu/dr)^2$.[76] For CO adsorbed on top, on bridge, and hollow sites of Pt_4 clusters, the IR intensity is enhanced by factors of 19, 8, and 6, respectively, compared to that of free CO (Table 3). It is convenient to decompose $d\mu/dr$ into σ and π components, $d\mu/dr = d\mu_\sigma/dr + d\mu_\pi/dr$, to separate σ and π channels of charge redistribution (Table 3).[77] When CO interacts with a Pt_4 cluster, the absolute values of the smaller positive σ and the larger negative π components of the dipole moment derivative increase significantly. As a result, the total dynamic dipole moment $d\mu/dr$ becomes more negative. Also, although the σ component of the dynamic dipole moment depends only slightly on the adsorption site, variations of the π component are significant. Similar results have previously been found for CO interacting with Pt atoms and model clusters of transition metal surfaces.[32,33,77]

The bonding analysis just presented deserves further comment, in particular with regard to the trends of various quantities when the adsorption site changes from on-top to bridge to 3-fold hollow. In that (canonical) order of sites, the bond distance $r(Pt_1-CO)$ increases, the intermolecular stretching frequency ω(Pt−CO) decreases, and the binding energy BE(CO) (Table 3) decreases, and these variations are consistent with one another. Another set of quantities that varies consistently among each other in the canonical series of sites are the bond distance r(CO) (increases), the red shift $\Delta\omega$(CO) (increases in absolute value), and the strength of the π back-donation as measured by the Mulliken population π(CO) (increases); see Tables 3 and 6. However, the two types of trends are, in a certain way, countercurrent to each other. Actually, the first set of quantities, which includes the CO adsorption binding energy, is at variance with the unmitigated donor−acceptor model of transition metal CO bonding,[67] since the interaction strength does not vary synchronously with the strength of π back-donation.[32,33,52]

The results of the CSOV analysis of on-top Pt−CO bonding mentioned above[52] allow a discussion of the calculated site variation of the CO binding energy. The size and relative weight of the four interaction contributions (Pauli repulsion, σ donation, π back-donation, and metal polarization) vary significantly with the different coordination situation of the various adsorption sites. These four contributions partially cancel each other. Therefore, accurate estimates are required for a prediction of the adsorption energy alteration with the coordination number of CO. (Looking ahead to the charged cluster models to be discussed in the subsequent section, we note that the alterations of many calculated quantities caused by changes of the cluster charge by ±1 au are significantly smaller than those resulting from a change in the adsorption site; see Table 3.) Obviously, as the present results demonstrate, the attempt to correlate the site variation of the adsorption energy with the strength of the back-donation *alone* is abortive. A comparative CSOV analysis of the three different adsorption sites of Pt_4/CO would be interesting but is outside the scope of the present study. To emphasize the danger of oversimplification when trying to correlate the adsorption energy with a single interaction channel, we refer to results for CO adsorption on the Ir_4 cluster.[78] In this system many computed properties, e.g., r(C−O), $\Delta\omega$(CO), $r(Ir_1-C)$, and ω(Ir−CO), vary for the different adsorption sites in a fashion similar to that reported here for the Pt_4/CO complexes. Nevertheless, the calculated energetically favored adsorption site for CO on Ir_4 is the bridge site, at variance with the on-top site for CO on Pt_4.

CO Adsorbed on Pt_4^+ and Pt_4^-. The positively charged Pt_4^+ species is formed from the neutral cluster Pt_4 by removing an electron from the orbital $27t_2$, which may be characterized by Mulliken populations as $s^{0.53}p^{0.34}d^{0.12}$. Electron abstraction is accompanied by a change of the effective electron configuration of the Pt atoms from $5d^{8.55}6s^{0.98}6p^{0.39}$ to $5d^{8.54}6s^{0.84}6p^{0.29}$ and results in the assigned electronic ground state $^4A_1$ (Tables 2 and 4). The corresponding electronic configurations and assigned ground states are summarized in Tables 2 and 3. Removal of an electron from the system Pt_4/CO results in the electronic configurations a_2e^2, b_1, and e^3 for the hollow, bridge, and on-top sites, respectively (Table 4). Pt_4^+/CO complexes where CO is adsorbed at the 3-fold hollow or the bridge site result in doublet states (^2E and $^2B_1$, respectively), whereas a quartet state $^4A_1$ was found in the case of CO bound to the on-top site.

Selected calculated parameters that characterize the interaction of a CO probe molecule with a charged Pt_4^+ cluster are collected in Table 3. The structural changes of the moieties Pt_4^+ and CO upon their interaction resemble those of the corresponding neutral systems and differ in most cases systematically from the latter (Table 3). The distance $r(Pt_1-C)$ is noticeably elongated for the on-top site but is almost unchanged when CO adsorbs on the bridge and hollow sites. For all adsorption configurations considered, the distance r(C−O) becomes shorter than in the corresponding Pt_4/CO complexes but remains still longer than in free CO. Concomitantly, the red shift of the C−O stretching frequency decreases by 30−100 cm^{-1} with respect to the values computed for Pt_4/CO (Table 3). As discussed in the previous section, the main factor that determines $\Delta\omega$(CO) is the charge redistribution in the π channel. The total Mulliken π population of CO when adsorbed on Pt_4^+ is reduced in comparison with the values for CO bound to Pt_4 (Table 6). All these results consistently point to a lower propensity of the positively charged platinum cluster (relative to neutral Pt_4) for donating electron density. This conclusion is corroborated by the eigenvalues of the highest occupied Kohn−Sham MO ϵ_{HOMO} = −10.1 and −4.6 eV for Pt_4^+ and Pt_4, respectively. The CO σ population remains almost unchanged when the Pt_4 cluster becomes ionized. Analysis of the CO dynamic dipole moment leads to the same conclusion (Table 3). Although the value $d\mu_\sigma/dr$ of Pt_4^+/CO displays only very limited alterations (less than 0.1 au) compared to the corresponding values of Pt_4/CO, considerably larger changes are found for the component $d\mu_\pi/dr$. The latter decreases (in absolute value) for a positively charged substrate Pt_4^+, indicating again less π back-donation than in the corresponding Pt_4/CO complexes. Reduced absolute values of $d\mu/dr$ imply less pronounced enhancements of the IR intensities of the C−O mode in the case of adsorption on the positively charged Pt_4^+ cluster.

For all configurations of the complex Pt_4^+/CO, from on-top to hollow CO coordination, all computed adsorption features

follow the same trends as found for the corresponding neutral complexes Pt_4/CO. In particular, the Pt_4^+−CO bond energy and the frequency ω(Pt−CO) are reduced compared to the values computed for the neutral system Pt_4/CO (Tables 3 and 5), but so are the π back-donation and the absolute value of the frequency shift $\Delta\omega$(CO). Apparently, for a given adsorption site, one can rationalize the charge-induced changes of both types of cluster properties (binding energy *and* frequency shift $\Delta\omega$(CO); see preceding section) by assuming that they are dominated by the change in the strength of the π back-donation, all other interactions remaining essentially unmodified.

We turn now to discussing the structure, binding, and vibrational properties of the adsorption complexes with CO bound to the Pt_4^- cluster. In the negatively charged Pt_4^- an additional electron occupies the orbital $27t_2$, altering the effective Mulliken configuration of the Pt atoms from $5d^{8.55}6s^{0.98}6p^{0.39}$ to $5d^{8.59}6s^{1.09}6p^{0.51}$; the assigned electronic state is $^6T_1$ (see Tables 2 and 4). Electronic states and configurations of the Pt_4^-/CO complexes are also reported in Tables 2 and 4. (We note in passing that the anionic cluster Pt_4^- is large enough so that its electronic structure may be calculated to reasonable accuracy with the exchange-correlation approximations used in the present study.[79]) Pt_4^-/CO complexes where CO is adsorbed at the 3-fold hollow site or at the on-top site result in doublet states ($^2A_1$ and $^2A_2$, respectively), whereas a sextet state $^6B_1$ was computed in case of CO bound to the bridge site (Table 2).

For Pt_4^-/CO in the on-top and bridge CO configurations, the interaction of the probe molecule with the substrate is stronger than in the corresponding neutral complexes Pt_4/CO. All adsorption properties reflect this effect (Table 3). Note in particular the enhanced values of the binding energy BE(CO), the frequency ω(Pt−CO), the red shift $\Delta\omega$(CO) (absolute value), the dynamic dipole moment and its components (absolute values), and the Mulliken population π(CO) (Tables 3 and 5). In these two coordinations, the negatively charged species Pt_4^- is apparently able to exert a stronger π back-donation than in the corresponding neutral cluster. Compare also the one-electron energies of the cluster HOMO: $\epsilon_{HOMO} = -0.4$ eV (Pt_4^-) and −4.6 eV (Pt_4). The bridge adsorption system of Pt_4^-/CO deserves further analysis. In this complex, the addition of the extra electron causes the complex to change from a doublet state ($^2B_1$ for neutral Pt_4/CO) to a sextet state ($^6B_1$ for Pt_4^-/CO); such a high-spin rearrangement is not observed in cases of CO adsorbed on top and at the 3-fold hollow sites (Table 3). The relatively strong interaction of the Pt_4 cluster with CO (and, in general, the interaction between a metal cluster and a ligand or substrate; see next section) is found to lead to partial spin quenching, in line with previous findings.[51] On the other hand, when electrons are added to the cluster Pt_4, the HOMO−LUMO gap is found to decrease because of increasing electron−electron interaction in rather localized d-type MOs. This in turn may lead to favoring a high-spin configuration, as is the case for the bridge adsorption system of Pt_4^-/CO. In the present study neutral and charged Pt_4/CO moieties are models for analogous systems adsorbed in a zeolite cage. Therefore, the corresponding cluster−substrate interaction is expected to lead to spin quenching rather than to an increase in the number of the uncoupled spins. For this reason we also studied the $^4A_2$ excited state generated by promoting one electron from the orbital $48b_1$ to the lowest unoccupied orbital $26a_2$. This excited state $^4A_2$ is calculated to be somewhat less stable than the corresponding cluster ground-state $^6B_1$ (Table 3) by only 0.24 and 0.34 eV at the LSD and BP//LSD levels, respectively. However, as displayed in Table 3, properties of adsorbed CO differ only in a minor fashion between the two states.

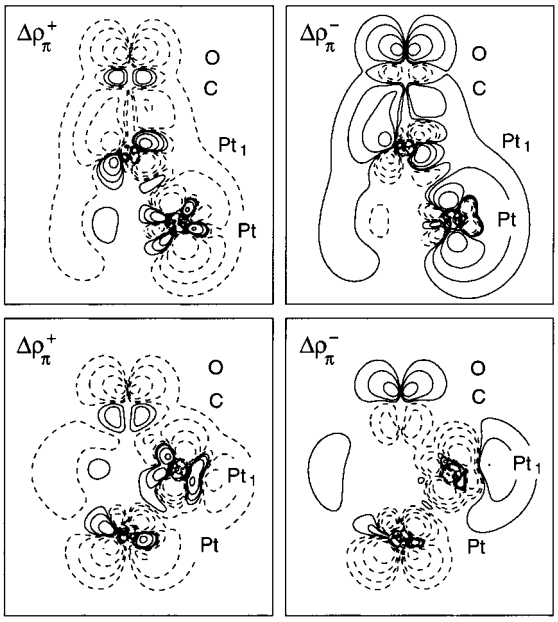

Figure 2. π-Electron density difference maps $\Delta\rho_\pi^+ = \rho_\pi(Pt_4^+/CO) - \rho_\pi(Pt_4/CO)$ (left panels) and $\Delta\rho_\pi^- = \rho_\pi(Pt_4^-/CO) - \rho_\pi(Pt_4/CO)$ (right panels). CO adsorbed on top (top panels) and on the hollow site (bottom panels). Solid and dashed lines indicate positive and negative values, respectively. The contours are drawn at ±0.03612, ±0.01, ±0.003612, and ±0.001 au.

At variance with CO adsorption at the on-top and bridge sites, the Pt_4^-−CO bond in the 3-fold hollow complex exhibits peculiarities: all computed properties of adsorbed CO are very close to those calculated for the neutral Pt_4/CO complex (Tables 3 and 5). This is in line with the value of the Mulliken population π(CO), which is quite similar to that of the neutral cluster Pt_4/CO.

Electron density difference maps can furnish a more direct picture of the charge redistribution that occurs when electronically modified Pt_4 clusters interact with the probe molecule CO. It is convenient to compare to the corresponding situations that involve neutral Pt_4/CO moieties. In Figure 2 density changes due to electron enrichment and depletion are displayed for both on-top and hollow site adsorption: $\Delta\rho_\pi^+ = \rho_\pi(Pt_4^+/CO) - \rho_\pi(Pt_4/CO)$ and $\Delta\rho_\pi^- = \rho_\pi(Pt_4^-/CO) - \rho_\pi(Pt_4/CO)$. In light of the preceding discussion only density changes in the π channel are presented. The map $\Delta\rho_\pi^+$ for CO on top indicates that the density of the missing electron is delocalized over the whole complex; particularly discernible is the charge depletion in the CO region. The map $\Delta\rho_\pi^+$ for CO adsorbed on the hollow site is rather similar. The density change $\Delta\rho_\pi^-$ for the complex Pt_4^-/CO with on-top CO is almost the negative of $\Delta\rho_\pi^+$ for that adsorption geometry. The plot shows that the extra electron is mainly distributed over the whole complex. Note the features in the CO region ($2\pi^*$ orbital) and near the Pt_1−CO bond. On the other hand, for CO adsorbed at the hollow site of Pt_4^-, the π charge density change in the CO region is less pronounced (only three contour lines) compared to the other three plots of Figure 2 (four contour lines). Furthermore, π charge density is depleted in the Pt_1−CO bonding region of the hollow Pt_4^-/CO system instead of the density accumulation found in the bonding region for on-top CO (see the corresponding map of $\Delta\rho_\pi^-$). This analysis shows that there is less π back-donation to CO adsorbed on the hollow site of the Pt_4^- cluster, in line with peculiar properties computed for this system (see Table 3 and

the preceding discussion). The electronic configurations of this system, e^4a_1, correspond to the addition of the extra electron in the orbital $46a_1$ (Table 2). This orbital has 60% sp character, and it is mainly located at the end of the Pt cluster opposite to the adsorbate. A charge density map of the orbital (not shown) clearly indicates that a small amount of the electron density is also distributed on the CO molecule through the σ channel and indeed cannot contribute to the lowering of the frequency of the CO stretching vibration (see Table 4). Therefore, in the same spirit as discussed, we also calculated the properties of the adsorption system in configuration e^4e (^{2}E), which is generated by promoting an electron from the orbital $46a_1$ to the lowest unoccupied orbital, 53e. The resulting ^{2}E electronic state of the hollow Pt_4^-/CO system is less stable than the $^2A_1$ cluster ground state by only 0.16 (LSD) and 0.22 eV (BP//LSD) (Table 3). In this case, the pertinent parameters are somewhat different, despite the small difference in stability of these two complexes. In particular, a more pronounced deformation of the intermetal distances is calculated as is a longer value for r(CO) (Table 3). Concomitant with the increased elongation of r(CO), an enhanced red shift is computed for the C−O stretching vibration, $\Delta\omega(CO) = -646$ cm^{-1} for the ^{2}E state in comparison with $\Delta\omega(CO) = -582$ cm^{-1}, calculated for the $^2A_1$ electronic ground state. This result is in line with an increased π(CO) population computed for this system (^{2}E) (Table 5). Orbital 53e, newly occupied in the ^{2}E state, exhibits similar sp character as orbital $46a_1$; inspection of contour maps (not shown) reveals that orbital 53e, different from $46a_1$, is partially delocalized onto the CO molecule through the π channel. Thus, promotion of an electron into the orbital can indeed affect the CO stretching frequency through increased back-donation.

Finally, we summarize in Figure 3 how selected calculated adsorption parameters, $\Delta\omega$(CO), ω(Pt−CO), and binding energy BE, of the complexes Pt_4/CO vary with the charge of the system. The binding energy of CO bound on top as well as at the bridge and hollow sites appears to be quite sensitive to the cluster charge. Its value increases for all coordination sites when the cluster charge becomes more negative. The intermolecular frequency ω(Pt−CO) exhibits a well-pronounced dependence on the cluster charge only for on-top CO. For CO adsorption at bridge and hollow sites, the alterations of the frequency ω(Pt−CO) do not exceed 25 cm^{-1}. For CO adsorbed on platinum clusters entrapped in a Na−X zeolite, the frequency ω(Pt−CO) is measured to increase by 60 cm^{-1} relative to the value observed for CO adsorbed at Pt(111) single crystals or films.[12] The value $\omega(Pt-CO) = 607$ cm^{-1} computed for Pt_4^-/CO (Table 3, Figure 3) is 133 cm^{-1} higher than that from DF calculations for CO adsorbed on the Pt(100) surface.[32] This result can be interpreted in two ways: (i) if one assumes the size of encapsulated platinum clusters studied in ref 12 to be comparable to that considered here, then one can deduce that less negatively charged platinum species are present in the cavities of the Na−X zeolite; (ii) alternatively, the observed shift $\Delta\omega$(Pt−CO) of 60 cm^{-1} may be attributed to the larger size of encaged platinum clusters that bear a considerable negative charge. The latter assumption is more consistent with the experimental data.[12]

The red shift of the C−O frequency for on-top, bridge, and hollow adsorption is also affected by the charge of the Pt_4 cluster; it increases in absolute size with decreasing charge (Figure 3). For CO adsorbed at the 3-fold hollow site, a linear correlation between $\Delta\omega$(CO) and the charge of the Pt cluster results only if the Pt_4^-/CO is represented in the excited electronic state ^{2}E (see above) (Figure 3 and Table 3). Bridged CO is only moderately affected by the charge of the cluster; $\Delta\omega$(CO) of

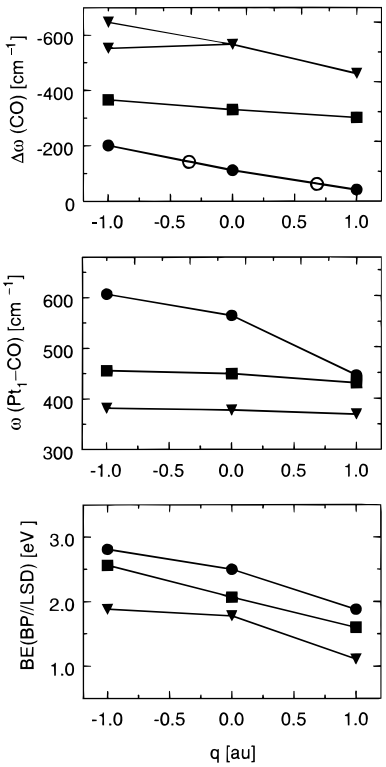

Figure 3. Dependence of computed properties of the complexes Pt_4/CO on the charge q of the cluster Pt_4^q (● on-top, ■ bridge, ▼ 3-fold site): frequency shift $\Delta\omega$(CO) (top panel); intermolecular frequency ω(Pt−CO) (middle panel); adsorbate binding energy BE(BP//LSD) (bottom panel). For the hollow Pt_4^-/CO complex, $\Delta\omega$(CO) obtained from the ^{2}E states is also displayed (see Table 3). Also shown are frequency shifts $\Delta\omega$(CO) (○) for CO adsorbed on top for noninteger values of q.

Pt_4^+/CO and of Pt_4^-/CO change by 20% in comparison with the value for Pt_4/CO. On the other hand, a much more pronounced variation of $\Delta\omega$(CO) is calculated for on-top CO (Figure 3 and Table 3). Direct comparison with experiment is not easy because observed IR bands are rather broad (100−200 cm^{-1}) and comprise a variety of peaks that correspond to CO molecules adsorbed on sites in different environments; metal particles of different sizes and shapes with different locations in the zeolite matrix lead to variations in the strength of metal−zeolite interactions. Lateral interactions between CO adsorbates also affect the detected IR peaks. Despite the complex nature of the experimentally studied situation, some trends are clearly discernible: ω(CO) moves gradually to lower energies when CO probe molecules are adsorbed on platinum clusters entrapped in Na−Y, Na−X, and Cs−X zeolites, which exhibit increasing basicity of the framework oxygen atoms.[3] The same trend was observed for CO adsorption on platinum clusters in alkali-exchanged L zeolites.[10] For Pt species in the more basic zeolites Cs−X and Cs−L, the red shift $\Delta\omega$(CO) is 40−50 cm^{-1} larger (in absolute value) in comparison to the red shift observed when CO is adsorbed on Pt particles supported on substrates such as SiO_2 or Al_2O_3.[3,10,62] On the other hand, C−O IR bands in the region 2090−2100 up to 2120 cm^{-1}, which are assigned to mononuclear Pt_1 species, were observed in acidic zeolites.[3−6,80−82] These observations show a reduction in the absolute value of the red shift $\Delta\omega$(CO) relative to the values of 2070−2080 cm^{-1} detected for CO adsorbed on Pt species, which are either supported on inert substrates or big enough to remain essentially unaffected by the zeolite framework.

CO Adsorbed on Na/Pt_4, Na^+/Pt_4, and NH_3/Pt_4. We turn now to a discussion of the chemical effects that the zeolite framework or nonframework atoms can exert on encapsulated Pt_4 clusters. So far, we have modeled these effects in a very approximate way by employing the models Pt_4^+ and Pt_4^-, i.e., by simply varying the electron count on the clusters. An improved model for such environment effects is to consider coordination of model electron-donor or electron-acceptor species X to the Pt_4 clusters. The NH_3 molecule and the Na atom were chosen to mimic charge-transfer X $\rightarrow$ Pt_4 to the cluster, and the cation Na^+ was taken to represent the electron donation by the cluster X $\leftarrow$ Pt_4. To restrict the computational effort, we chose 3-fold hollow coordination of the X groups (Figure 1). These interactions have been analyzed in terms of the electronic structure change of Pt_4 clusters and of the adsorption-induced changes of the vibrational parameters of the CO probe molecule. The electronic configuration and assigned state of all systems discussed in this section are reported in Tables 2 and 3.

When a Na atom or a Na^+ cation is bound to the Pt_4 cluster, the latter undergoes a charge redistribution as indicated by the changes in the intramolecular Pt−Pt distances and by the Mulliken populations (Table 6). In the system Na/Pt_4 the distance r(Pt−Pt) = 2.536 Å slightly elongates in comparison with r(Pt−Pt) = 2.508 Å computed for free cluster Pt_4, whereas in the complexes Na^+/Pt_4 the distance r(Pt−Pt) = 2.487 Å is somewhat shorter. Concomitantly, a Na atom acquires a positive charge and Na^+ reduces its positive charge, as a manifestation of the charge transfer that occurs toward or from the Pt_4 cluster, respectively. When the molecule NH_3 is coordinated to the fragment Pt_4, only very moderate modifications of the intramolecular Pt−Pt distances have been computed. This finding implies that the charge transfer from the NH_3 molecule toward the Pt_4 cluster is rather small (if any). Also, the value of the binding energy computed for the system NH_3/Pt_4 at the LSD level is very small; at the BP level the system is not bound. The electronic configuration of the system $a_2e^2e^1$ resembles that of the free Pt_4 cluster (Tables 2 and 3), in line with the fact that the adsorbate is only very weakly bound. Mulliken charges do not match these observations, since a more positive charge is computed for NH_3 than for Na (Table 6). This is an example where a Mulliken analysis is not suitable for evaluating the amount of charge transfer between two fragments of a system. Note that the 3-fold site of transition metal clusters is calculated to be energetically less favorable for adsorption of an ammonia molecule than the on-top site.[83] Therefore, the on-top configuration of an ammonia-cluster adsorption complex may be a more realistic model than the presently considered system μ_3-NH_3/Pt_4.

The electron density difference map $\Delta\rho_{Na} = \rho(Na/Pt_4) - \rho(Pt_4) - \rho(Na)$ (Figure 4) clearly shows a charge-transfer Na $\rightarrow$ Pt_4. The computed properties of a CO probe molecule bound to the Na/Pt_4 fragment, r(C−O) = 1.165 Å, $\Delta\omega$(CO) = −146 cm^{-1}, ω(Pt−CO) = 583 cm^{-1}, lie between the corresponding values calculated for the complexes Pt_4/CO and Pt_4^-/CO (Tables 3 and 6). These results also indicate that the probe molecule CO interacts with an electron-enriched platinum moiety bearing an effective charge between 0 and −1 au. Not unexpectedly, the map $\Delta\rho_{Na}{}^+ = \rho(Na^+/Pt_4) - \rho(Pt_4) - \rho(Na^+)$ shows a charge redistribution from the Pt_4 cluster to Na^+ (Figure 4). In an analogous fashion, when a CO molecule is attached to the moiety Na^+/Pt_4, all computed properties of the adsorbed CO, r(C−O) = 1.148 Å, $\Delta\omega$(CO) = −64 cm^{-1}, ω(Pt−CO) = 529 cm^{-1}, lie between the corresponding values calculated for the complexes Pt_4/CO and Pt_4^+/CO (Tables 3 and 6). In this case the probe molecule CO obviously interacts with an electron-deficient platinum substrate, which is characterized by an effective charge between 0 and +1 au. A similar result has been calculated for CO adsorbed on the cluster Mg^{2+}/Ir_4.[84]

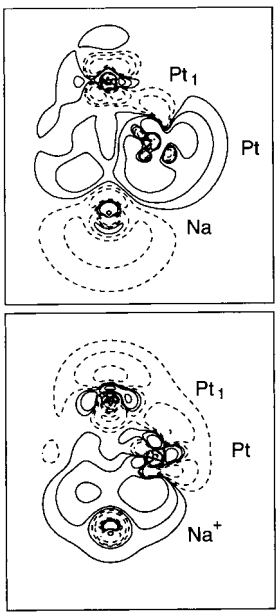

Figure 4. Electron density difference maps $\Delta\rho_X = \rho(X/Pt_4) - \rho(Pt_4) - \rho(X)$ with X = Na (top panel) and X = Na^+ (bottom panel). Solid and dashed lines indicate positive and negative values, respectively. The contours are drawn at ±0.01, ±0.003612, ±0.001 au.

As noted above, the cluster NH_3/Pt_4 is somewhat different from the clusters Na/Pt_4 and Na^+/Pt_4. All properties of CO adsorbed on the cluster NH_3/Pt_4, r(C−O) = 1.158 Å, $\Delta\omega$(CO) = −116 cm^{-1}, ω(Pt−CO) = 547 cm^{-1}, are very similar to those computed for the complex Pt_4/CO (Tables 3 and 6). This is not surprising, given the very weak interaction of NH_3 with the substrate Pt_4 (Table 6). The molecule NH_3 is a rather strong base,[85] yet its interaction with the 3-fold hollow site of the Pt_4 fragment affects the electronic structure and other parameters of the cluster only insignificantly. This implies that only those centers in zeolites that exhibit very strong basic properties are able to notably alter the electronic structure and adsorption features of entrapped metal clusters; this conclusion should be even more appropriate for substantially larger clusters than Pt_4 considered here.

The linear correlation between the frequency shift $\Delta\omega$(CO) of CO adsorbed on top and the charge q of the cluster Pt_4 displayed in Figure 3 suggests the following analysis. By use of this linear relationship, effective charge values of the Pt_4 cluster in Na/Pt_4 and Na^+/Pt_4 can be deduced from the calculated frequency shifts of Na/Pt_4/CO, $\Delta\omega$(CO) = −146 cm^{-1}, and Na^+/Pt_4/CO, $\Delta\omega$(CO) = −64 cm^{-1}. Not unexpectedly, these effective charges signal partial reduction or oxidation of the metal moiety: −0.35 au (Na/Pt_4) and +0.68 au (Na^+/Pt_4). We have also computed the properties of CO adsorbed on the model clusters $Pt_4^{-0.35}$ ($t_1{}^3t_2{}^{1.35}$) and $Pt_4^{+0.68}$ ($t_1{}^3t_2{}^{0.32}$) with fractional charges to elaborate the meaning of these estimated charges and to check whether a linear relationship between the adsorption-induced shift of the C−O frequency and the charge of the Pt_4 species, caused by electron-donor or -acceptor substituents, indeed exists. Remarkable agreement is found between calculated bond distances and vibrational frequencies of the target and model complexes Na/Pt_4/CO and $Pt_4^{-0.35}$/CO, as well as Na^+/Pt_4/CO and $Pt_4^{+0.68}$/CO (Table 6). The agreement of

calculated binding energies is less satisfactory (Table 6). As discussed above, $\Delta\omega$(CO) is mainly affected by the amount of back-donation and by the ability of the metal cluster to donate electron charge. On the other hand, the binding energy results from a delicate balance of several contributions (Pauli repulsion, σ donation, π back-donation, metal substrate polarization), which is obviously altered when the physical nature of the metal cluster that interacts with the CO probe is modified. Such changes occur in the electronically modified Pt_4^q cluster models that mimic electron-donating or -accepting substrates that interact with the metal cluster.

From this result we conclude that transition metal clusters with a modified charge constitute appropriate models for describing vibrational properties of metal moieties in electronic states that are affected by interactions with donor and acceptor species. Moreover, the linear correlation between the charge of the Pt_4 cluster and the frequency shift $\Delta\omega$(CO) of CO adsorbed on top suggests that for metal particles of a given size, the C−O frequency shift can be used to estimate the charge of electron-enriched or electron-deficient metal particles present in zeolite hosts. For instance, from the correlation chart displayed in Figure 3, a red shift $\Delta\omega$(CO) of -40 cm^{-1} and a blue shift of 20 cm^{-1} (both values lie in the range observed for CO adsorbed on Pt_n species in basic and acidic zeolites)[3] would imply that the CO probe molecules interacts with clusters of effective charge -0.3 or $+0.3$ au, respectively, if one can assume Pt_4 species to be present. Of course, the electronic effect of a zeolite host on larger entrapped metal particles will be less pronounced (and consequently, adsorption properties will be changed to a lesser degree) because the electron redistribution will take place over a larger particle volume.

Conclusions

In this work we focused on the characterization of vibrational properties of a CO probe adsorbed on Pt_4 clusters, which were intended to model small platinum species entrapped in zeolite cavities. We calculated various properties of the substrate clusters and the adsorption systems with the help of a scalar-relativistic density functional method. Electronically modified clusters were considered to mimic the metal−support interaction; a positively charged Pt_4^+ moiety was taken to represent electron-deficient metal species formed because of the influence of an electron-attracting support (e.g., an acidic zeolite), and a negatively charged Pt_4^- species was used to model electron-enriched metal particles that are stabilized in the presence of hosts with electron-donor capability (e.g., framework oxygen anions in basic zeolites).

For CO adsorbed on top of the neutral cluster Pt_4, the calculated C−O frequency ω(CO) is red-shifted compared to free CO by 112 cm^{-1} and by 331 and 556 cm^{-1} for CO on the bridge and 3-fold hollow sites of Pt_4, respectively. This trend was ascribed to increased back-donation when the CO probe interacts with ever more Pt atoms of the cluster. The C−O stretching frequency turned out to be quite sensitive to the charge of the Pt_4 cluster; a linear correlation was found between the shift $\Delta\omega$(CO) and the cluster charge. Although for CO adsorbed on the bridge site of Pt_4^- and Pt_4^+ clusters ω(CO) varies only by 20% in comparison with the values computed for the neutral complex Pt_4/CO, a much more pronounced variation was calculated for on-top and hollow CO. For CO adsorbed at the on-top site, the energetically preferred adsorption geometry, this correlation was utilized to estimate the effective charge values of metal particles as induced by interaction with their surrounding. Such environmental effects were studied for Pt_4 clusters interacting with Na and Na^+ species that were employed to mimic the effect of an electron-donating or -attracting support, respectively. The properties of CO adsorbed on Na/Pt_4 and on Na^+/Pt_4 were computed to be very close to those for CO bound to the appropriately charged clusters Pt_4^q ($q = -0.35, +0.68$ au), where the charge had been determined from the calculated correlation. These electronically modified clusters indeed often constitute good models for describing electron-enriched or electron-deficient states of small platinum particles as induced by metal−support interaction. CO molecules were found to probe the charge of the metal clusters by means of the frequency ω(CO), irrespective of how this particular state has been generated, either by directly modifying the (partial) charge of the cluster or by charge exchange resulting from a substituent/support attached to the cluster.

Although the intermolecular frequency ω(Pt−CO) for CO adsorbed on top was also calculated to be quite sensitive to the electronic state of the metal cluster, no linear correlation with the cluster charge similar to that of ω(CO) was found.

Work is under way to extend the present investigation to larger platinum clusters in order to study the effect of cluster size on bonding and vibrational properties of CO probe molecules as well as to characterize the sensitivity of these observables to cluster charge modifications in the case of larger metal particles.

Acknowledgment. This work has been supported by the Deutsche Forschungsgemeinschaft and the Fonds der Chemischen Industrie.

References and Notes

(1) Gates, B. *Catalytic Chemistry*; Wiley: New York, 1992.
(2) Sachtler, W. M. H.; Zhang, Z. *Adv. Catal.* **1993**, *39*, 129.
(3) Barthomeuf, D. *Catal. Rev.* **1996**, *38*, 521.
(4) Sachtler, W. M. H. *Acc. Chem. Res.* **1993**, *26*, 386.
(5) Stakheev, A. Y.; Shpiro, E. S.; Tkachenko, O. P.; Jaeger, N. I.; Schulz-Ekloff, G. *J. Catal.* **1997**, *169*, 382.
(6) McCarthy, T. J.; Marques, C. M. P.; Treviño, H.; Sachtler, W. M. H. *Catal. Lett.* **1997**, *43*, 11.
(7) Stakheev, A. Y.; Shpiro, E. S.; Jaeger, N. I.; Schulz-Ekloff, G. *Catal. Lett.* **1995**, *32*, 147.
(8) Khodakov, A.; Barbouth, N.; Oudar, J.; Villain, F.; Bazin, D.; Dexpert, H.; Schulz, P. *J. Phys. Chem. B* **1997**, *101*, 766.
(9) Vaarkamp, M.; Modica, F. S.; Miller, J. T.; Koningsberger, D. C. *J. Catal.* **1993**, *144*, 611.
(10) Han, W.-J.; Kooh, A. B.; Hicks, R. F. *Catal. Lett.* **1993**, *18*, 193.
(11) Kappers, M. J.; Van der Maas, J. H. *Catal. Lett.* **1991**, *10*, 365.
(12) Kazansky, V. B.; Borovkov, V. Y.; Sokolova, M.; Jaeger, N. I.; Schulz-Ekloff, G. *Catal. Lett.* **1994**, *23*, 263.
(13) Kustov, L. M.; Ostgard, D.; Sachtler, W. M. H. *Catal. Lett.* **1991**, *9*, 121.
(14) Besoukhanova, C.; Guidot, J.; Barthomeuf, D.; Breysse, M.; Bernard, J. R. *J. Chem. Soc., Faraday Trans. 1* **1981**, *77*, 1595.
(15) Weber, W. A.; Gates, B. C. *J. Phys. Chem. B* **1997**, *101*, 10423.
(16) Kawi, S.; Chang, J. R.; Gates, B. C. *J. Phys. Chem.* **1993**, *97*, 10599.
(17) Kawi, S.; Gates, B. C. *J. Phys. Chem.* **1995**, *99*, 8824.
(18) Deutsch, S. E.; Miller, J. T.; Tomishige, K.; Iwasawa, Y.; Weber, W. A.; Gates, B. C. *J. Phys. Chem.* **1996**, *100*, 13408.
(19) Marchese, L.; Boccuzzi, M. R.; Coluccia, S.; Lavagnino, S.; Zecchina, A.; Bonneviot, L.; Che, M. In *Structure and Reactivity of Surfaces*; Morterra, C., Zecchina, A., Costa, G., Eds.; Studies in Surface Science and Catalysis 48; Elsevier: Amsterdam, 1989; p 653.
(20) Barshad, Y.; Zhou, X.; Gulari, E. *J. Catal.* **1985**, *94*, 128.
(21) Primet, M. *J. Catal.* **1984**, *88*, 273.
(22) De Mallmann, A.; Barthoumeuf, D. In *Zeolites as Catalysts, Sorbents and Detergent Builders*; Karge, H. G., Weitkamp, J., Eds.; Studies in Surface Science and Catalysis 46; Elsevier: Amsterdam, 1989; p 429.
(23) Shpiro, E. S.; Tuleuova, G. J.; Zaikovskii, V. I.; Tkachenko, O. P.; Vasina, T. V.; Bragin, O. V.; Minachev. K. M. In *Zeolites as Catalysts, Sorbents and Detergent Builders*; Karge, H. G., Weitkamp, J., Eds.; Studies in Surface Science and Catalysis 46; Elsevier: Amsterdam, 1989; p 143.
(24) Stakheev, A. Y.; Sachtler, M. H. *J. Chem. Soc., Faraday Trans. I* **1991**, *87*, 3703.

(25) Phuong, T. T.; Massardier, J.; Gallezot, P. *J. Catal.* **1986**, *102*, 456.
(26) Dunlap, B. I.; Rösch, N. *Adv. Quantum Chem.* **1990**, *21*, 317.
(27) Rösch, N.; Krüger, S.; Mayer, M.; Nasluzov, V. A. In *Recent Development and Applications of Modern Density Functional Theory. Theoretical and Computational Chemistry*; Seminario, J. M., Ed.; Elsevier: Amsterdam, 1996; Vol. 4, p 497.
(28) Belling, T.; Grauschopf, T.; Krüger, S.; Nörtemann, F.; Staufer, M.; Mayer, M.; Nasluzov, V. A.; Birkenheuer, U.; Rösch, N. *ParaGauss1.19*; Technische Universität: Munich, 1998.
(29) Rösch, N.; Krüger, S.; Belling, T.; Nörtemann, F.; Staufer, M.; Zenger, C.; Grauschopf, T. In *HPSC97—Stand und Perspektiven des Parallelen Höchstleistungsrechnens*, Proceedings of the Statustagung des BMBF, Munich, February 1997; Wolf, H., Krahl, R., Eds.; DLR: Berlin; p 165.
(30) Belling, T.; Grauschopf, T.; Krüger, S.; Mayer, M.; Nörtemann, F.; Staufer, M.; Zenger, C.; Rösch, N. In *High Performance Scientific and Engineering Computing*, Proceedings of the First International FORTWIHR Conference, Munich, 1998; Bungartz, H.-J., Durst, F., Zenger, C., Eds.; Lecture Notes in Computational Science and Engineering; Springer: Heidelberg, in press.
(31) Gropen, O. *J. Comput. Chem.* **1987**, *8*, 982.
(32) Chung, S. C.; Krüger, S.; Pacchioni, G.; Rösch, N. *J. Chem. Phys.* **1995**, *102*, 3695.
(33) Pacchioni, G.; Chung, S. C.; Krüger S.; Rösch, N. *Surf. Sci.* **1997**, *392*, 173.
(34) Van Duijneveldt, F. B. IBM Research Report No. RJ 945; IBM Corporation, 1971.
(35) Neyman, K. M.; Strodel, P.; Ruzankin, S. P.; Schlensog, N.; Knözinger, H.; Rösch, N. *Catal. Lett.* **1995**, *31*, 273.
(36) Veillard, A. *Theor. Chim. Acta* **1968**, *12*, 405.
(37) Heiz, U.; Vayloyan, A.; Schumacher, E.; Yeretzian, C.; Stener, M.; Gisdakis, P.; Rösch, N. *J. Chem. Phys.* **1996**, *105*, 5574.
(38) Pople, J. A.; Gill, P. M. W.; Johnson, B. G. *Chem. Phys. Lett.* **1992**, *199*, 557.
(39) Gill, P. M. W.; Johnson, B. G.; Pople, J. A. *Chem. Phys. Lett.* **1993**, *209*, 506.
(40) Nasluzov, V. A.; Rösch, N. *Chem. Phys.* **1996**, *210*, 413.
(41) Vosko, S. H.; Wilk, L.; Nusair, M. *Can. J. Phys.* **1980**, *58*, 1200.
(42) Becke, A. D. *Phys. Rev. A* **1988**, *38*, 3098.
(43) Perdew, J. P. *Phys. Rev. B* **1986**, *33*, 8622; **1986**, *34*, 7406 (E).
(44) *Recent Development and Applications of Modern Density Functional Theory*. *Theoretical and Computational Chemistry*; Seminario, J. M., Ed.; Elsevier: Amsterdam, 1996; Vol. 4.
(45) Fan, L.; Ziegler, T. *J. Chem. Phys.* **1991**, *95*, 7401.
(46) Boys, S. F.; Bernardi, F. *Mol. Phys.* **1970**, *19*, 553.
(47) Dai, D.; Balasubramanian, K. *J. Chem. Phys.* **1995**, *103*, 648.
(48) Wyckoff, R. W. G. *Crystal Structures*, 2nd ed.; Interscience Publishers: New York, 1965; Vol. 1.
(49) Häberlen, O. D.; Chung, S. C.; Stener, M.; Rösch, N. *J. Chem. Phys.* **1997**, *106*, 5189.
(50) Krüger, S.; Vent, S.; Rösch, N. *Ber. Bunsen-Ges. Phys. Chem.* **1997**, *101*, 1640.
(51) Pacchioni, G.; Rösch, N. *Acc. Chem. Res.* **1995**, *28*, 390.
(52) Illas, F.; Zurita, S.; Márquez, A. M.; Rubio, J. *Surf. Sci.* **1997**, *376*, 279.
(53) Ogletree, D. F.; van Hove, M. A.; Somorjai, G. A. *Surf. Sci.* **1982**, *123*, 264.
(54) Philipsen, P. H. T.; van Lenthe, E.; Snijders, J. G.; Baerends, E. J. *Phys. Rev. B* **1997**, *56*, 13556.
(55) Ibach, H.; Mills, D. L. *Electronic Energy Loss Spectroscopy and Surface Vibrations*; Academic Press: New York, 1982.
(56) Sheppard, N.; Nguyen, N. T. *Adv. Infrared Raman Spectrosc.* **1978**, *5*, 67.
(57) Hayden, B. E.; Bradshaw, A. M. *Surf. Sci.* **1983**, *125*, 787.
(58) Steineger, H.; Lehwald, S.; Ibach, H. *Surf. Sci.* **1982**, *123*, 264.
(59) Klünker, C.; Balden, M.; Lehwald, S.; Daum, W. *Surf. Sci.* **1996**, *360*, 104.
(60) Thiel, P. A.; Behm, R. J.; Norton, P. R.; Ertl, G. *J. Chem. Phys.* **1983**, *78*, 7448.
(61) Ruett-Robey, J. E.; Doren, D. J.; Chabal, Y. J.; Christman, S. B. *Phys. Rev. Lett.* **1988**, *61*, 2779.
(62) Brandt, R. K.; Hughes, M. R.; Bourget, L. P.; Truszkowska, K.; Greenler, R. G. *Surf. Sci.* **1993**, *286*, 15.
(63) Primet, M. *J. Catal.* **1984**, *88*, 273.
(64) Primet, M.; de Menorval, L. C.; Fraissard, J.; Ito, T. *J. Chem. Soc., Faraday Trans. 1* **1985**, *81*, 2867.
(65) Bischoff, H.; Jaeger, N. I.; Schulz-Ekloff, G.; Kubelkova, L. *J. Mol. Catal.* **1993**, *80*, 95.
(66) Huber, K. P.; Herzberg, G. *Constants of Diatomic Molecules*; Van Nostrand Reinhold: New York, 1979.
(67) Blyholder, G. *J. Phys. Chem.* **1964**, *68*, 2772.
(68) Andzelm, J.; Salahub, D. R. *Int. J. Quantum Chem.* **1986**, *29*, 1091.
(69) Görling, A.; Ackermann, L.; Lauber, J.; Knappe, P.; Rösch, N. *Surf. Sci.* **1993**, *286*, 26.
(70) Hu, P.; King, D. A.; Lee, M. H.; Payne, M. C. *Chem. Phys. Lett.* **1995**, *246*, 73.
(71) Bauschlicher, C. W., Jr.; Bagus, P. S. *J. Chem. Phys.* **1984**, *81*, 5889.
(72) Pacchioni, G.; Bagus, P. S. *J. Chem. Phys.* **1990**, *93*, 1209.
(73) Bagus, P. S.; Hermann, K.; Bauschlicher, C. W., Jr. *J. Chem. Phys.* **1984**, *81*, 1966.
(74) Illas, F.; Zurita, S.; Rubio, J.; Márquez, A. M. *Phys. Rev. B* **1995**, *52*, 12372.
(75) Bagus, P. S.; Illas, F.; Sousa, C.; Pacchioni, G. In *Electronic Properties of Solids using Cluster Models*; Kaplan, T. A., Torphe, M. F., Eds.; Fundamental Material Science I; Plenum: New York, 1994.
(76) Amos, R. D. *Adv. Chem. Phys.* **1987**, *67*, 99.
(77) Hermann, K.; Bagus, P. S.; Bauschlicher, C. W., Jr. *Phys. Rev. B* **1984**, *30*, 7313.
(78) Ferrari, A. M.; Neyman, K.; Rösch, N. Unpublished.
(79) Rösch, N.; Trickey, S. B. *J. Chem. Phys.* **1997**, *106*, 8940.
(80) Barshad, Y.; Zhou, X.; Gulari, E. *J. Catal.* **1985**, *94*, 128.
(81) Lane, G. S.; Miller, J. T.; Modica, F. S.; Barr, M. K. *J. Catal.* **1993**, *141*, 465.
(82) Zholobenko, V. L.; Lei, G. D.; Carvill, B. T.; Lerner, B. A.; Sachtler, W. M. H. *J. Chem. Soc., Faraday, Trans. 1* **1994**, *90*, 233.
(83) Neyman, K. M.; Staufer, M.; Nasluzov, V. A.; Rösch, N. *J. Mol. Catal. A* **1996**, *119*, 245.
(84) Jansen, A. P. J.; van Santen, R. A. *J. Phys. Chem.* **1990**, *94*, 6764.
(85) Cotton, F. A.; Wilkinson, G. *Advanced Inorganic Chemistry*, 4th ed.; Wiley-Interscience: New York, 1980.